Final Draft

of the original manuscript

Scheider, I.; Barbini, A.; dos Santos, J.:

Numerical residual strength prediction of stationary shoulder friction stir welding structures.

In: Engineering Fracture Mechanics. Vol. 230 (2020) 107010.

First published online by Elsevier: 28.03.2020

https://dx.doi.org/10.1016/j.engfracmech.2020.107010

Numerical Residual Strength Prediction of Stationary Shoulder Friction Stir Welding Structures

I. Scheider, A. Barbini, J.F. dos Santos

Institute of Materials Research, Materials Mechanics, Helmholtz-Zentrum Geesthacht

Abstract:

The residual strength of a structure made of dissimilar Aluminium panels joined by a stationary shoulder friction stir welding (SS-FSW) process is predicted by numerical simulation using finite elements including cohesive elements for crack propagation. The yield strength and strain hardening parameters within the stir zone and adjacent thermos-mechanically affected and heat affected zones are derived from a tensile specimen cut out from the panel perpendicular to the weld seam. The identification is conducted by a hybrid numerical/experimental procedure with an inverse search by help of digital image correlation in order to get the strain field at the welded surface and to compare them to the numerical calculation. The crack propagation parameters are retrieved from specimens with crack in the stir zone and heat affected zone on either side. After this identification procedure, the fracture behaviour of a coupon specimen with a crack crossing the weld is predicted.

Keywords: residual strength, cohesive zone model, welded structures, parameter identification, stress-strain curve

Introduction

The integrity assessment of welded structures has been a scientific topic for decades due to the material property changes close to the weldment and the corresponding critical performance of the complete structure, see e.g. the review in [1]. Often cracks already exist in this area and extend easily due to the decreased fracture resistance in this region, or they start somewhere else and propagate in an unstable manner as soon as growing cracks reach a weld region and lead to sudden failure of the structure. The sources for the occurrence of cracks are manifold:

- The welding process leads to rapid solidification of the material in the weld seam and microstructural changes in its neighbourhood. Due to that treatment, the fracture resistance is often drastically reduced, particularly in the heat-affected zone.
- A sub-optimal welding process may lead to hot-cracking and pores, that is, micro cracks already exist even before the structure is in service.
- The different texture regions have particular material properties, commonly denoted as strength mismatch. This affects the local stresses in the weld region and may increase any crack tip stresses.
- The welding residual stresses may also increase the local stress level. However, this effect is usually compensated by the plasticity occurring in residual strength tests and is therefore of minor importance here.

The integrity assessment must take all these factors into account; particularly, scenarios of an existing crack must be considered for approved reliability of a structure. In principle, there are two different scenarios, in which the problems due to crack propagation and failure in weld joints may occur:

1. Cracks which are already existing within (or close to) the weld seam, are initiating and propagating. Since they are already located in the neighbourhood of a rather brittle region like the heat affected zone, unstable crack growth is more likely and dangerous for the stability of the whole structure.

2. If a crack originates from some other position and propagates towards a weld seam, the crack propagation may become unstable when it approaches the heat affected zone.

While the first scenario has often been investigated experimentally as well as analytically and numerically, e.g. [2-6], the second has been reported only a few times, see e.g. [7, 8], even though the latter touches a case which is important for the certification of aerospace structures, the so-called two-bay crack of airplane fuselages. For this test, a crack is inserted axially in a fuselage skin. In this standard test, the crack advances in axial direction towards the circumferential stiffener (frame) upon internal pressure and in-plane tension loading, see Figure 1.

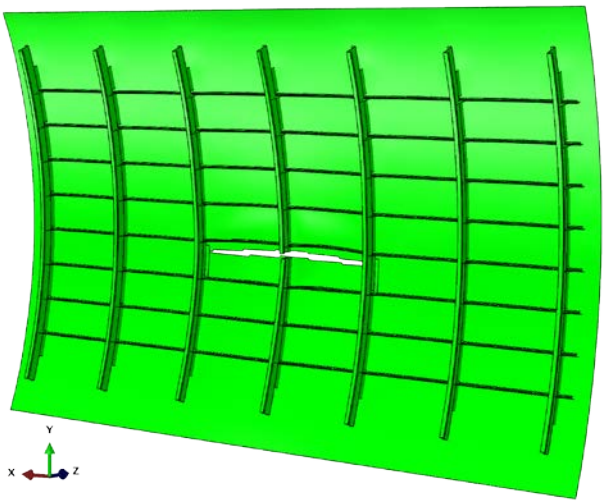

Figure 1: Finite element model of an airplane fuselage with a so-called two-bay crack, in which one frame is already broken, the crack approaches the two neighbouring stiffeners, from [9].

Traditionally, such so-called skin-stringer connections are produced using rivets. If a crack approaches the rivet joint, it propagates along the skin without degrading the stiffener, and the stiffener holds the cracked body together, see Figure 2. Contrarily, in an integral structure the crack will propagate in the skin and also in the stringer; it might also debond the stringer due to the stress concentration and reduced fracture toughness in the weld joint. Thus, a riveted structure has additional crack stopping mechanisms compared to a welded connection, and the welded connection must be understood well in order to take advantage from the weight savings and processing speed-up that generally come with the integral structure.

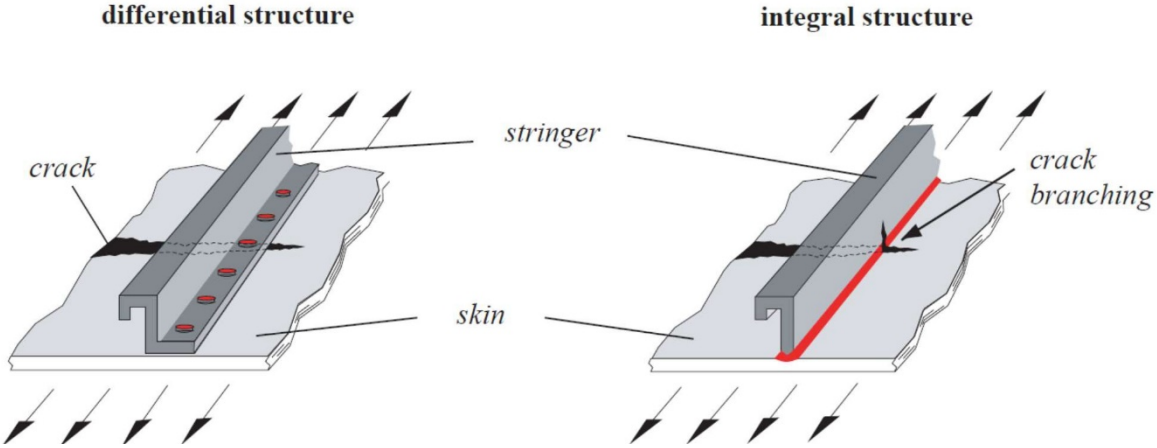

Figure 2: Crack propagation in a skin-stringer connection. Comparison between differential (riveted) structural (left) and integral (welded) structure (right), from [10]

The welding technique used here is a particular version of the friction stir welding (FSW), which is characterized by a non-rotating tool shoulder, the so-called *stationary-shoulder friction stir welding* (SSFSW) [11]. The tool for this technique consists of two parts, the pin and the shoulder, and only the pin which penetrates the material, is rotating, while the shoulder is fixed, see Figure 3(a). This leads to a change in the thermo-mechanically affected zone (TMAZ), and the weld seam has a symmetric shape. A comparison between the resulting cross section of the FSW and the SSFSW process is shown by the micrographs in Figure 3(b) (FSW) and (c) (SSFSW).

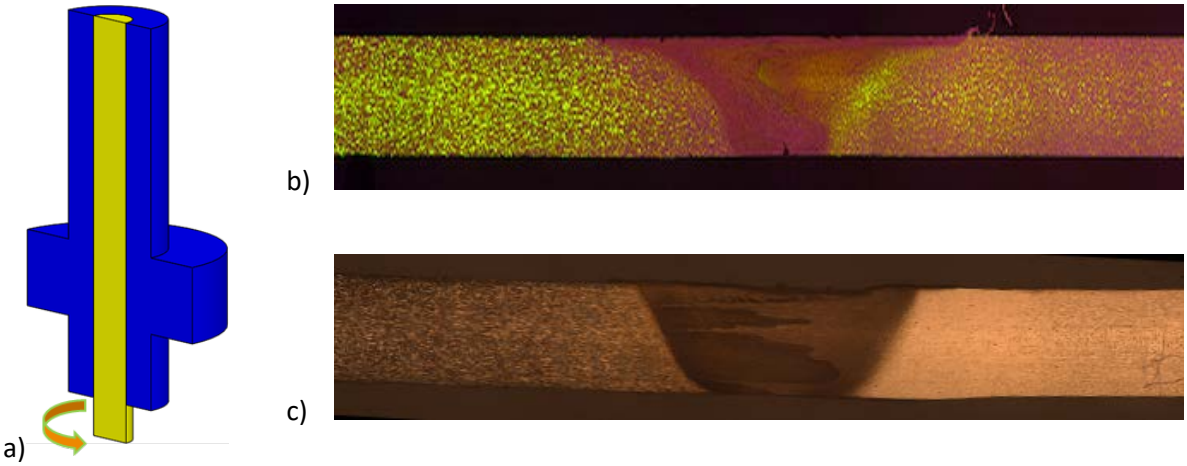

Figure 3: Left (a): Tool for the SSFSW process. Right: Cross sectional micrograph for two different weldments. (b) traditional FSW, (c) SSFSW.

For the structural assessment of an aircraft fuselage, particularly the skin-stringer connection, several idealization levels have been defined, see e.g. [12]. The most complex test is the barrel test, in which a complete segment of the fuselage is loaded under internal pressure. The second one is the panel testing, which contains (integral or riveted) stiffeners and frames. Types of panels can be divided in two groups: curved panels as shown in Figure 2, which can also be loaded by internal pressure, but then the test is almost as expensive as the barrel test. The second type is a straight panel, which is loaded under tension only. A typical representation is the five-stringer panel, see the principal sketch in Figure 4(a). The third level is the coupon level, where only the material and possibly the weldment is tested in a simple fracture specimen configuration, Figure 4(b). This is the level, which is investigated in the present study.

Due to the high complexity of real world structures, which includes 3D thin-walled geometry and several material regions, analytical assessment procedures have been used for a long time. Numerical assessment methods for weld joints using damage and crack extension simulation became popular in the last decade of the 20th century for simpler specimens, mainly using the following numerical methods:

- Crack propagation analyses using the cohesive zone model are employed for predefined extension directions [4, 5].
- Local approaches have often been employed using variants of the Gurson model (e.g. [2, 3, 6]), with which also the crack propagation direction can be estimated,
- CTOA methods have also been used for residual strength prediction, e.g. in [13], if the crack propagation direction is known.

A comprehensive review on these methods is given in [14]. Since the 21st century, crack path deviation has been modelled using X-FEM as well, see e.g. [15].

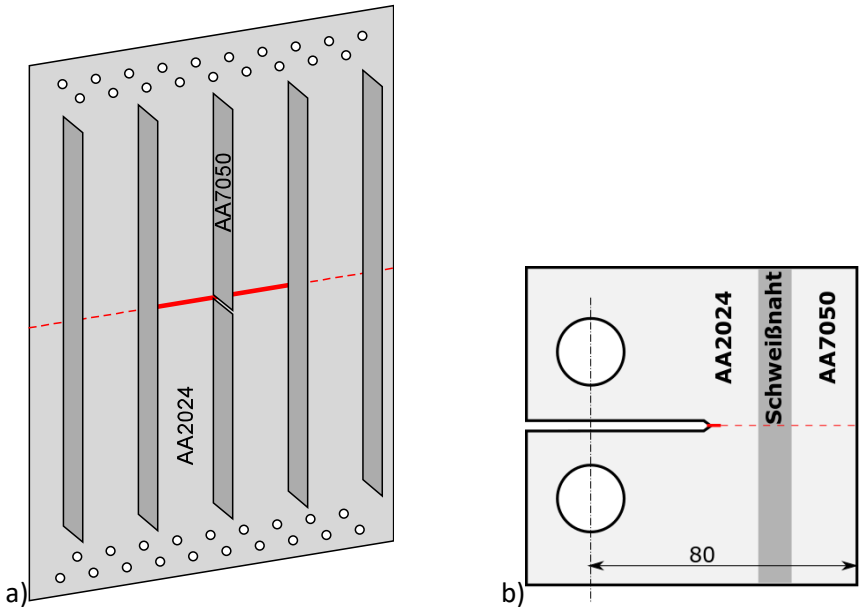

Figure 4: Idealization levels for an aircraft fuselage: a) five-stringer panel, b) C(T) specimen for testing the crack extension, crack direction approaching the weld joint. The dashed red line marks the crack propagation direction in the simulation using the cohesive zone model.

In this investigation, we aim at simulating a welded structure with a crack propagation direction perpendicular to weld line numerically by use of the cohesive zone model, Figure 4(b), supported by a number of experiments for parameter identification and validation. The reason for using the cohesive zone model is its ease of use, limited number of parameters and robustness even for large crack propagation [16]. The material and processes used here have been investigated by the co-authors experimentally already, see [17, 18].

The investigation is divided in three parts. Firstly, the elastic-plastic material behaviour in the neighbourhood of the weld joint is identified. Secondly, the crack propagation parameters for the cohesive zone model are identified at several positions across the weldment. In the third part, the simulation of the coupon test shown in Figure 4(b) is modelled with these parameters and validated against experiments in order to show the capabilities with respect to a reasonable residual strength prediction.

Identification of the yielding behaviour in the neighbourhood of the weld joint

In order to predict the crack propagation behaviour with high accuracy, the stress state in the vicinity of the crack tip must be calculated appropriately. Even though the engineering approach requires simple material models, plasticity is significant and must be taken into account. Here, von Mises plasticity will be considered with isotropic hardening, which is sufficient for residual strength prediction. In any case, the identification of the strain hardening behaviour in the weld region is of particular interest for the current study and the method to be used for its identification will thus be explained in detail.

Base material

The material used here is a combination commonly used for fuselage skin and stiffener. For the skin, a material is used, which is strong, reliable and available in large quantities, here the Aluminium AA2024 in heat treatment condition T3. The rolled sheet has a thickness of 2 mm. A high strength alloy AA7050 in T651 heat treatment condition is used for the stiffener material. Usually this material comes as an

extruded profile. For the present investigation, a rolled and heated material has been used in order to be able to produce larger test specimens.

For the yield curve of the base materials AA2024 and AA7050, tensile tests have been conducted using flat tensile specimens in longitudinal, diagonal and transverse direction. The specimens have a cross section of 2 x 12.5 mm and a gauge length of 50 mm. Tests have been conducted displacement controlled under quasi-static loading conditions with a displacement rate of 1 mm/min. Details of the test can be found in [18].

The AA7050 material does not have any direction dependence, while AA2024 has a lower yield strength in transverse direction, see Figure 5. As an approximation of the hardening law, a Voce type hardening is often used for Aluminium alloys [19], which is based on an exponential function with a maximum stress asymptote:

$$\sigma = \sigma_0 + (\sigma_\infty - \sigma_0)\left(1 - \exp\left(-\frac{\varepsilon_{pl}}{\varepsilon_0}\right)\right) \tag{1}$$

The functional form of the stress strain curves are plotted together with the experimental data using the parameters given in Table 1.

Table 1: Yield parameters for the base material

	initial yield strength $\sigma_0\ [MPa]$	ultimate yield strength $\sigma_\infty\ [MPa]$	reference strain $\varepsilon_0\ [-]$
AA7050 T651	535	660	0.0706
AA2024 T3 longitudinal	371	609	0.0973
AA2024 T3 transversal	351	618	0.106
AA2024 T3 diagonal	354	612	0.1082

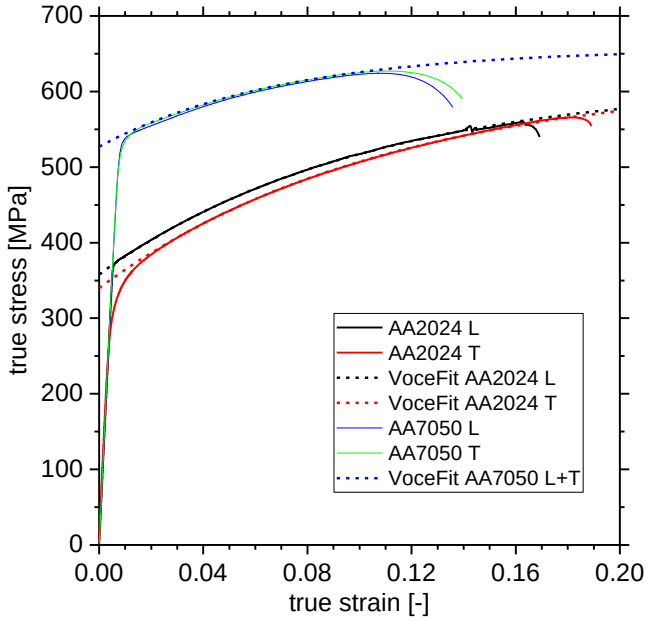

Figure 5: True stress-strain curves for AA2024 T3 and for AA7050 T7651, in transverse and longitudinal direction, respectively. Solid lines represent averaged experimental data, dashed lines the stress calculated by eq. (1) with the parameters from Table 1.

Weld region

In [17, 18] the effect of welding process parameters on the performance of the structural behaviour has been investigated thoroughly. It turned out that the optimal configuration is the one with AA2024 on the advancing side (the rotation direction of the tool is in the same direction as the welding itself), AA7050 is thus on the retreating side. The optimal welding speed has been found to be 3 mm/s. The identification of the stress-strain curve in welded regions, which can be used as an input for the simulation, is difficult since the material properties show large gradients. These gradients are also visible in the hardness distribution of the material, which has been measured by an array of micro hardness tests across the weld region cross section, see Figure 6. It turns out that the region left of the weld centre, that is, towards the AA2024 base material, features the lowest hardness value. On the other hand, the gradient in thickness direction (vertically) is rather small.

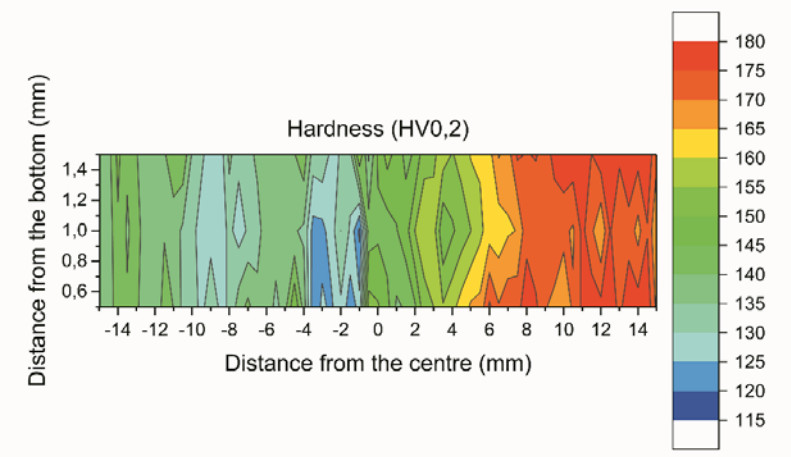

Figure 6: Hardness distribution across the weld cross section.

The yield strength changes proportional to the hardness, but the correlation between these two is not accurate enough to be used for the identification of the yield stress and hardening from the hardness distribution. Therefore the yield stress must be measured directly. Commonly, a multi-specimen method is used, see, e.g. [20, 21], for which a number of small specimens is taken from the different regions across the weld. The accuracy depends mainly on the size of the specimen and the number of sub-specimens taken over the relevant area. For the thin-walled panels used here, it is very difficult to produce specimens for small-scale tensile tests, and the testing procedure is challenging and time consuming. Therefore, a method will be presented in the following, with which the stress-strain behaviour of the whole region can be estimated by testing a single specimen taken orthogonal to the weld. The method consists of a combination of experiment and numerical simulation, and the main idea is based on the use of the surface strain field across the weld, which can be measured in-situ using digital image correlation (DIC). Under the assumption of a homogeneous stress state during the test (in each direction) one can calculate the stress at each material point. Thus, the in-plane strain and the normal stress is known in the whole specimen. The main principle has been used by Reynolds and Duvall in 1999 [22] already, who measured the strain at three points (weld centre and heat affected zone left and right) and plotted the stress (=F/A) over the local strain. However, the relation between stress and local strain in loading direction can only be used as the characteristic stress-strain curve, if the stress state is uniaxial, which is not the case if the material properties have a gradient. The strain gradient in loading direction results in strain gradients in lateral direction, which are constraint by the neighbouring material regions, causing a multiaxial stress state.

The strain field measured experimentally is shown in Figure 7(a). For the evaluation of the stress strain curves, the strain in loading direction is evaluated along the red line at three different load stages,

which are marked in the experimental force-displacement plot, Figure 7(b). For the numerical simulation, the stress-strain curve is taken at two sampling points, which are marked by the blue lines in Figure 7(c). At these points the stress-versus strain relation is approximated by eq. (1). As an input, a position dependent plasticity model is defined, in which the 3 parameters of eq. (1) are varying linearly across the weld region. For the FEM solver ABAQUS® this is conducted by user subroutine UHARD.

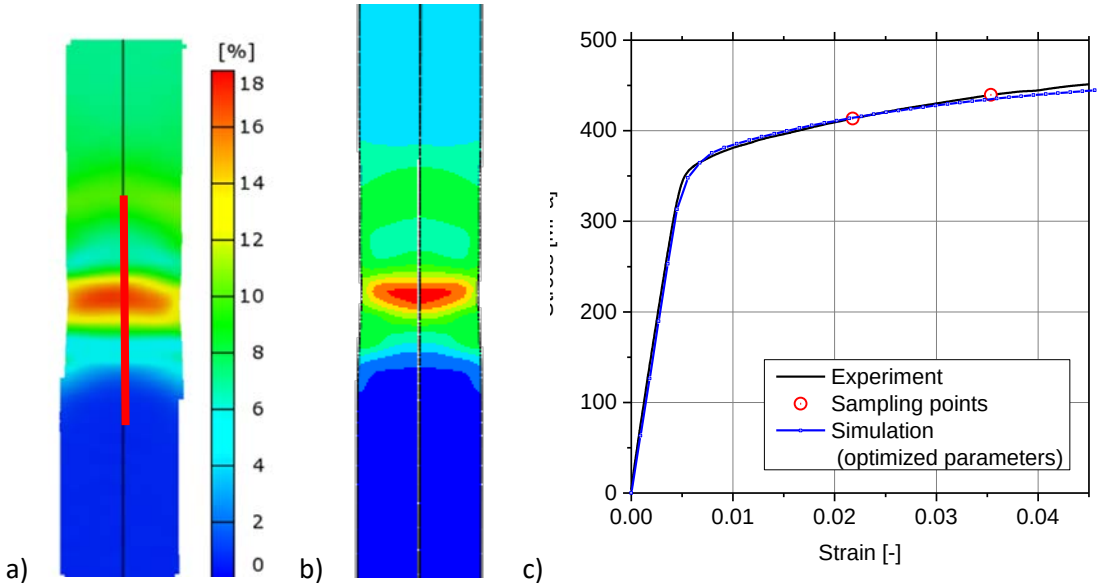

Figure 7: (a) Experimental strain measurement using DIC in the welded specimen. (b) Finite element simulation of the same region with optimized parameters, see below. (c) Force-displacement curve of the tensile test with three markers where the strain has been evaluated.

As explained above, the difference between experiment and simulation using the position dependent yielding is large, if the relation between nominal stress (=F/A) and local normal strain are taken as input for a finite element simulation without correction. The error is visualized in Figure 8(a) by a comparison between the experimental and numerical strain distribution along the evaluated line.

In order to get a better agreement between experiment and simulation with respect to the strain field in the specimen, we optimize the stress-strain curves at the specific points, keeping the linear variation between the sampling points. After the optimization, which has been conducted using a python script including the *optimize* module from *scipy* [23], the strain distribution across the weld region is also shown in Figure 8(a). The parameters used eventually are plotted in Figure 8 (b). All further simulations have been conducted with this set of parameters.

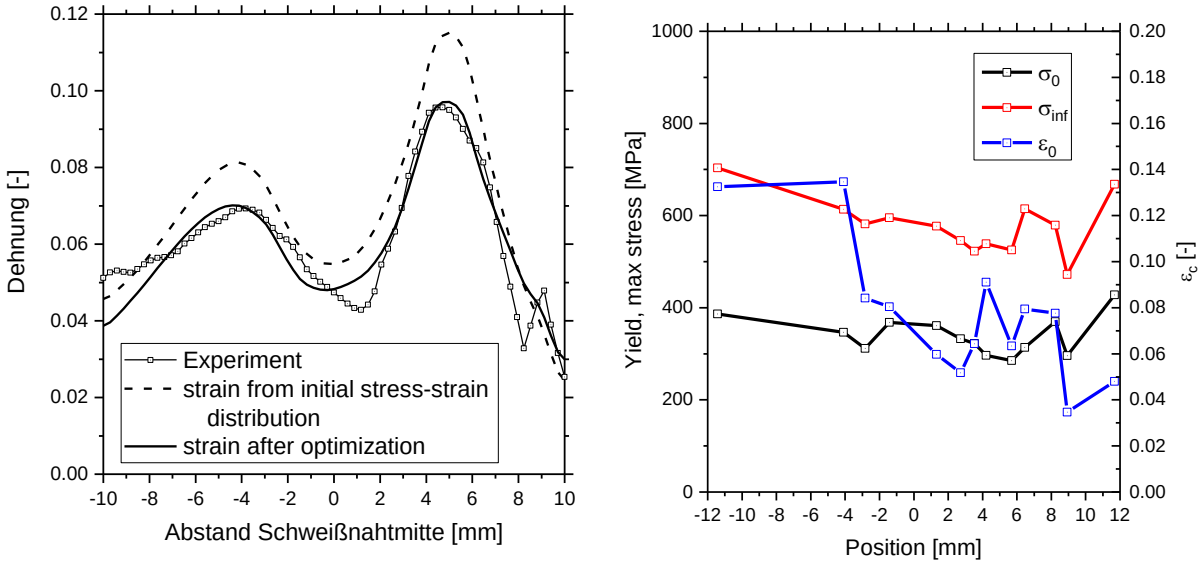

Figure 8: (a) Difference between measured and finite element strain distribution along the red line shown in Figure 7(a), before and after the optimization. (b) Variation of the stress-strain parameter from eq. (1) after optimization.

Identification of the crack propagation parameters

Fundamentals and base material identification

The cohesive zone model (CZM) is being used for the simulation of crack propagation and assessment of residual strength. For the CZM, the fracture process zone ahead of the crack tip is being idealized by an interface with zero thickness, in which the damage and failure occurs, while the rest of the structure behaves damage-free. In the current simulations, pure mode I crack propagation is considered, that is, the crack propagation direction is known beforehand. For this kind of fracture, the constitutive behaviour of the CZM is a relation between the normal stress, in the following denoted as traction, acting on the interface, T, and the material separation, δ, it is thus called the *traction-separation law* (TSL). In general, it has two parameters, the cohesive strength, T_0, and the separation energy, Γ_0. For the shape of the function $T(\delta)$, many different functions have been proposed. We have a large experience with a shape that contains a constant stress regime,

$$T = T_0 \begin{cases} 2\left(\frac{\delta}{\delta_1}\right) - \left(\frac{\delta}{\delta_1}\right)^2 & \delta < \delta_1 \\ 1 & \delta_1 \le \delta < \delta_2 \\ 2\left(\frac{\delta-\delta_2}{\delta_0-\delta_2}\right)^3 - 3\left(\frac{\delta-\delta_2}{\delta_0-\delta_2}\right)^2 + 1 & \delta_2 \le \delta < \delta\_0 \end{cases}, \qquad (2)$$

see the graph of the shape in Figure 9. This TSL has been implemented as a user element in ABAQUS® [24]. In contrast to the cohesive elements already included in the ABAQUS element library, these elements can handle the thickness change in plane stress structures.

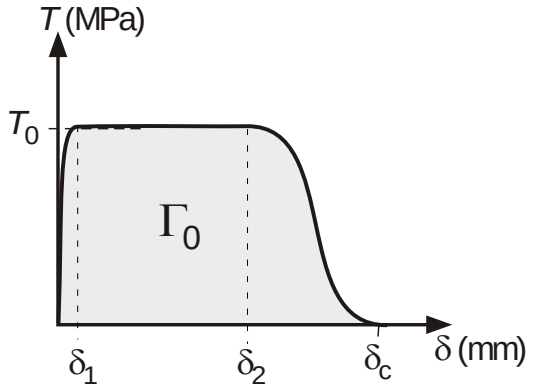

Figure 9: Traction-separation law of the cohesive zone model for pure mode I loading.

Based on previous simulations [25, 26] and our cohesive zone model user guide [16], we choose $\delta_1 = 0.01\,\delta_0$, $\delta_2 = 0.5\delta_0$ for all simulations. The separation energy is calculated as the integral of the traction over the separation, $\Gamma_0 = \int_0^{\delta_0} T(\delta)\,\mathrm{d}\delta$. For the shape given by eq. (**2**), the integral can be solved analytically, and the separation energy is $\Gamma_0 = T_0\delta_0\left[\frac{1}{2} - \frac{1}{3}\frac{\delta_1}{\delta_0} + \frac{1}{2}\frac{\delta_2}{\delta_0}\right]$. As a consequence, instead of the separation energy, the critical separation, δ_0, can also be the second parameter for the cohesive zone model.

The parameters T_0, Γ_0 must be identified for both base materials together with their variation within the weld region and the TMAZ/HAZ. For their identification, fracture mechanics tests with specimens containing cracks in the different regions of the structure are reproduced by finite element simulations using 2D plane stress elements for the panel itself and cohesive elements along the prospective crack path. Centre cracked panels M(T)200 with $2a_0 = 70\,\mathrm{mm}$ have been used for the AA2024 base material, and compact tension C(T)50 specimens with $a_0 = 25\,\mathrm{mm}$ for the AA7050 base material. The identification is based on a fitting procedure adjusting the two cohesive model parameters such that the numerical force-displacement curve meets the experimental one. Based on existing investigations with AA2024T3, see [25], initial values for the optimisation have been set to $T_0 \approx 800$ MPa and $\Gamma_0 \approx 10$ kJ/m². The identification follows a very simple but reliable trial-and-error approach not discussed further; the final parameters of this optimization are rather given in Table 2.

Weld region

For the welding region, it would be optimal to have a parameter distribution with a high number of sampling points similar to the stress-strain curve, but this is not possible, since the crack path is not completely straight if the crack originates in the HAZ, but rather kinks into the least resistant regions. Three configurations could be tested, all with a crack parallel to the welding direction. One is a crack in the weld centre, and another two configurations are for the crack in the advancing and retreating side, respectively. For these welded structures, M(T)200 specimens have been produced with an initial centre crack of $2a_0 = 74\,\mathrm{mm}$. In contrast to the base material M(T) specimens, where double symmetry has been utilized, only one symmetry plane is available in these specimens. In addition, the fine meshed region must me large enough to capture the material gradients across the weld region. The finite element mesh is shown in Figure 10. This mesh has been used for all three configurations (crack in weld centre, advancing and retreating side), the yield stress distribution has been shifted vertically by 5 mm with respect to the mesh instead. The detail in Figure 10 shows the distribution together with the meshing strategy in the welded region for the crack in the stir zone.

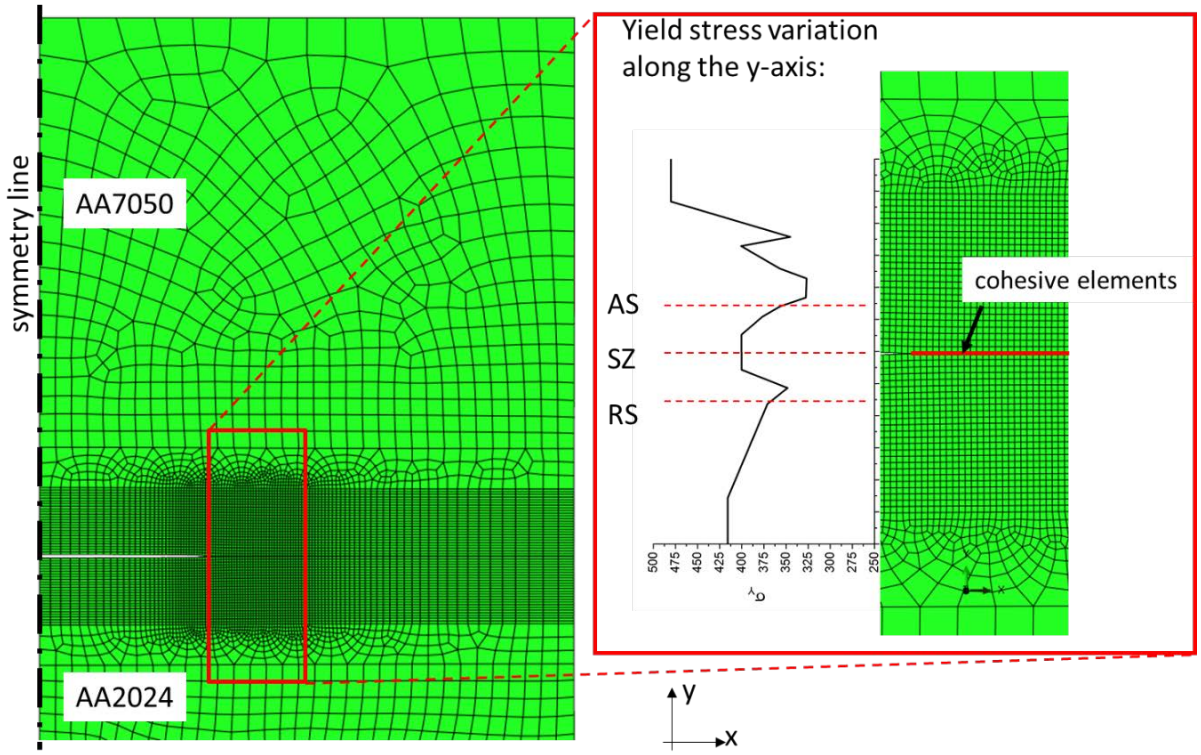

Figure 10: FE mesh of the welded M(T)200 panel (detail showing the right side of the panel, only). The cohesive element layer and the yield stress distribution for a crack in the stir zone [SZ] is shown on the right).

As for the base material, the cohesive model parameters have been adjusted such that the experimental force-displacement curves are reproduced by the simulations. The results are given in Figure 11. The parameters for the three configurations are given in Table 2 together with the base material data.

Table 2: Cohesive model parameters for base materials and three weld region configurations

	AA2024 base material	HAZ advancing (AA2024) side	Stir zone	HAZ retreating (AA7050) side	AA7050 base material
Cohesive strength [MPa]	850	1070	980	1000	1100
Separation energy [kJ/m²]	10	11	15	12	12

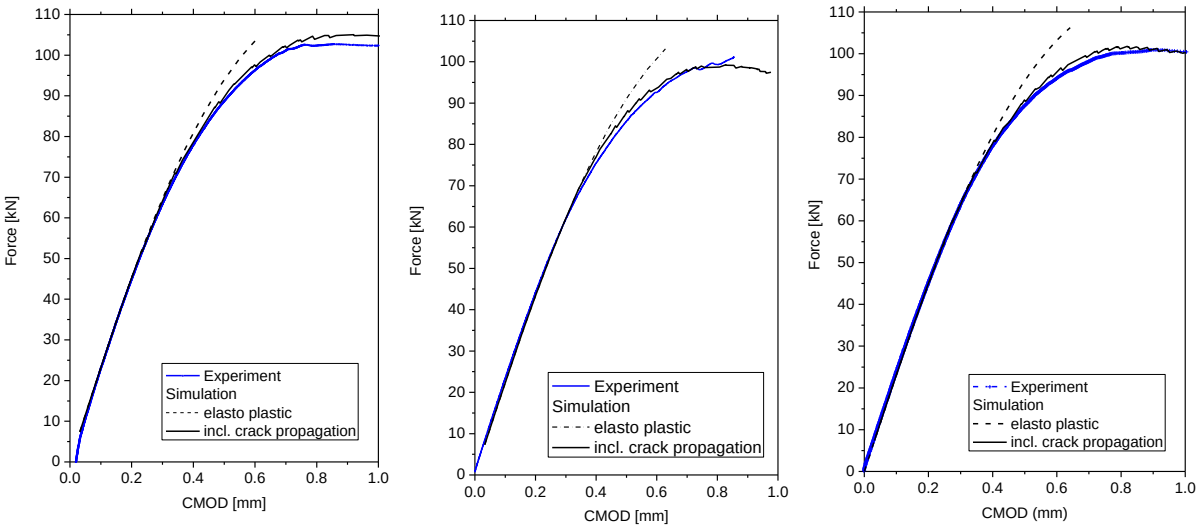

Figure 11: Force displacement curves for three configurations: left: Crack in the weld centre; middle: crack on the retreating (AA7050) side; right: Crack on the advancing (AA2024) side.

Residual strength prediction of a structure with crack perpendicular to the weld joint

Thanks to the preceding parameter identification procedure, at this point all parameters necessary for the validation have been collected. Now all these parameters are used to model the C(T) specimen shown in Figure 4(b). Since the cohesive parameters have been identified at three positions in the weld region only, while the yield behaviour is changing with a strong fluctuation, an approach for the interpolation between the given values must be used. Without any knowledge based assumption, a linear interpolation is used for the sake of simplicity. It is assumed that the influence of the process on the base material properties is ±12 mm. The resulting variation of the cohesive model parameters is plotted in Figure 12.

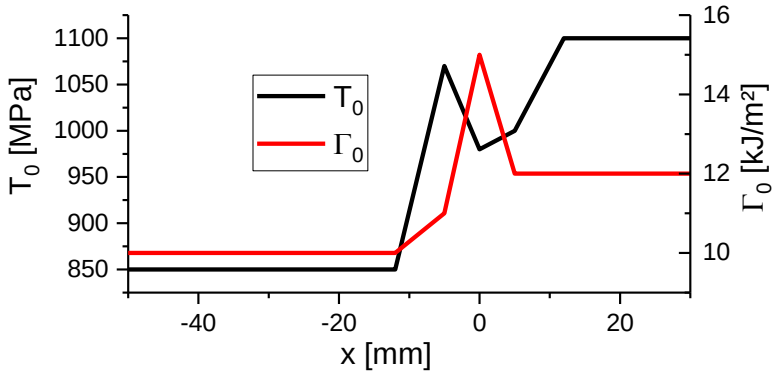

Figure 12: Variation of the cohesive properties in the weld region (x=0: centre of the stir zone)

The comparison of the numerical and the experimental force-displacement curves is shown in Figure 13(a). It turns out that the prediction of a maximum load (=residual strength) of$F_{\max}^{FE} = 4219\ N$ is lower than the actual experimental residual strength, which is $F_{\max}^{exp} = 4424\ N$, that is, 5% higher than the anticipated value. Contrarily, the numerically calculated fracture resistance, which is shown in Figure 13(b), is higher than the experimental one, which is also shown in the Figure. Both, the numerical and the experimental results use the same procedure for the identification of the crack driving force, *J*. Therefore, at a given displacement, the numerical *J* value is smaller than the one calculated from the experiment. One can conclude that the crack extension must be significantly larger

in the experiment compared to the simulation in order to give a lower *J*-R curve. Several explanations can be given for this discrepancy:

- The texture in the stir zone and the HAZ is not isotropic, but direction dependent, therefore, the cohesive parameters cannot be transferred from the identification, where the crack propagates in welding direction, to the validation, where the crack runs perpendicular.
- The proposed variation of the cohesive parameters in Figure 12 is not accurate enough to capture the real gradients accurately.
- The crack length measurement has been conducted by a multi specimen method. Since the stir zone has a gradient also in thickness direction, the crack length is not constant across the specimen. This variation has neither been measured experimentally nor taken into account in numerical simulations.

Summarising the sources of error, the agreement is in the range of expectations.

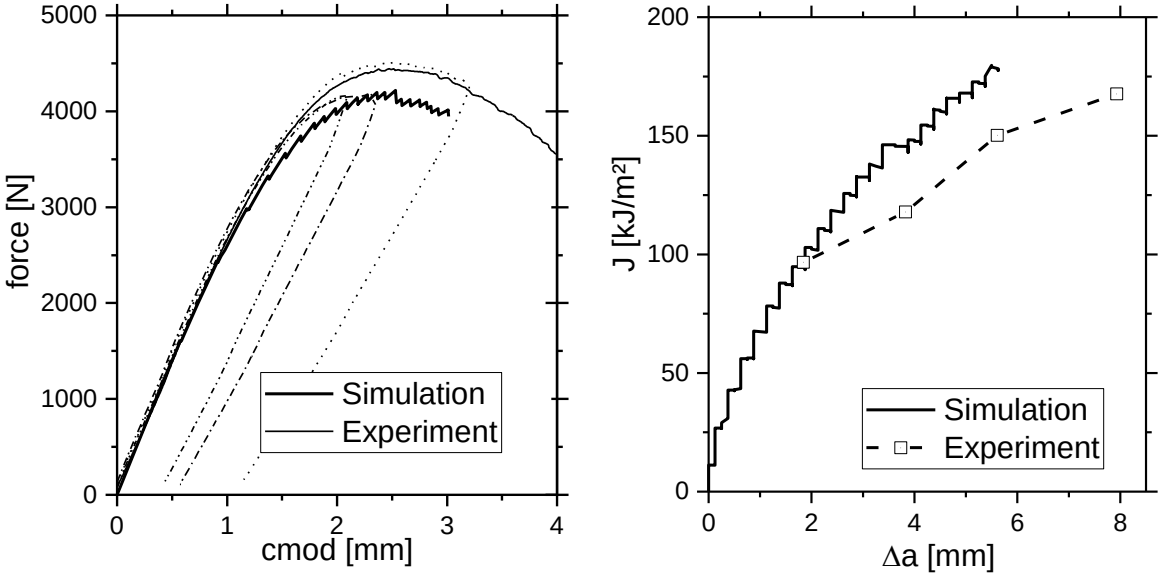

Figure 13: Results of the test on a welded C(T) specimen as shown in Figure 3(b) with a crack approaching the weld region. a) Force displacement curve; b) Crack resistance curve.

Conclusion and outlook

The residual strength assessment of weld joints is commonly quantified by testing a welded specimen with a crack within the weld region (either in the stir zone or in the HAZ), parallel to the welding direction. Only few investigations have been published on the crack propagation for cracks approaching the weld line. In the present study, a new method was developed to characterise the fracture behaviour of structures with rather simple experiments which nevertheless are useful for identifying the local material properties within the weld region. Under the assumption that the parameters are not anisotropic, which of course is a strong assumption particularly for sheet material properties, one can identify the complete field of all plasticity and crack propagation properties in the sheet. The approach can be summarised as a 4-step procedure:

1. Identification of the yielding behaviour for the base material(s), with tests in different directions, if necessary. No FE simulations are required.
2. Identification of the crack propagation behaviour of the base material(s) by standard fracture specimens. Finite element simulations are necessary to fit the cohesive model parameters to the experiment. These can be conducted in different directions as well.

3. Testing of cross-weld tensile specimens using DIC to examine the complete strain field across the weld region. The stress is assumed to be homogeneous and unidirectional in order to calculate an initial yield curve distribution. The number of free parameters depends on the number of parameters per yield curve (here we have used a three parameter Voce approximation) and the number of sampling points across the weld region. These parameters are then adjusted by an optimization procedure including finite element simulations.
4. Testing of a number of fracture specimens with initial cracks in the direction of the weld at different positions in the weld or the heat affected zone. The parameters for each specimen is identified by fitting the results of the numerical crack propagation analysis to the experiment.

The advantages of this procedure are:

- the material consumption for the parameter identification is minor,
- the testing facilities needed are reasonable (the DIC equipment for surface strains is the only major experimental investment),
- the models for the finite element simulations are usually small, that is, the computation time for one simulation is small, and
- the number of simulations depends on the quality required for the parameter identification.

The investigation showed that the parameter identified by this procedure can also be used to calculate the crack propagation for configurations, where the crack runs in a different direction (here: perpendicular to the weld instead of in the welding direction). The approach can be used as long as the crack propagation direction is predictable such that the cohesive elements can be placed in one layer.

An additional benefit of this investigation is the identification of a complete yield stress variation across the weld region with one specimen. Even though the strains for different positions are limited by the applied stress, the common assumption of a prescribed yield curve shape makes extrapolation for these regions possible.

As an outlook, the residual strength of a welded 5-stringer panel as shown in Figure 4(a) will be tested and simulated in order to check the applicability even for other weld configurations – the T-joint of a skin-stringer connection will definitely bring in further challenges compared to a butt joint.

In addition, one might also try to find the cohesive parameters with one precracked specimen with the crack approaching the weld joint, i.e., the specimen that is here used for validation might also be used for parameter identification instead. However, the testing procedure might be more difficult, since the crack propagation must be captured accurately to identify the different weld zones appropriately.

Acknowledgments

This work has been carried out within the scope of the Research Platform “Light-weight Assessment, Computing and Engineering Centre” (ACE Centre) as part of the reference project Lightweight Integral Structures for Future Generation Aircrafts (LISA). The help of Jan Carstensen during the preparation of the manuscript is gratefully acknowledged.

References

1. Zerbst, U., et al., *Review on fracture and crack propagation in weldments – A fracture mechanics perspective.* Engineering Fracture Mechanics, 2014. **132**: p. 200-276.
2. Schmitt, W. and D.Z. Sun, Blauel, J.G., *Damage mechanics analysis (Gurson model) and experimental verification of the behaviour of a crack in a weld-cladded component.* Nucl. Eng. Des., 1997. **174**: p. 237-246.

3. Nègre, P., D. Steglich, and W. Brocks, *Crack extension in aluminium welds: a numerical approach using the Gurson-Tvergaard-Needleman model.* Eng. Fract. Mech., 2004. **71**(16-17): p. 2365-2383.
4. Lin, G., et al., *The effect of strength mis-match on mechanical performance of weld joints.* Int. J. Fract., 1999. **96**: p. 37-54.
5. Tu, H.Y., S. Schmauder, and U. Weber, *Simulation of the fracture behavior of a S355 electron beam welded joint by cohesive zone modeling.* Engineering Fracture Mechanics, 2016. **163**: p. 303-312.
6. Tu, H.Y., et al., *Simulation of the damage behaviour of electron beam welded joints with the Rousselier model.* Engineering Fracture Mechanics, 2013. **103**: p. 153-161.
7. Miyazaki, N. and M. Nakagaki, *Two-dimensional finite element analysis of stably growing cracks in inhomogeneous materials.* International Journal of Pressure Vessels and Piping, 1995. **63**(3): p. 249-260.
8. Bhat, S. and S. Narayanan, *A computational model and experimental validation of shielding and amplifying effects at a crack tip near perpendicular strength-mismatched interfaces.* Acta Mechanica, 2011. **216**(1): p. 259-279.
9. Cornec, A., et al., *Application of the cohesive model for predicting the residual strength of a large scale fuselage structure with a two-bay crack.* Eng. Fail. Anal., 2009. **16**: p. 2541-2558.
10. Seib, E., *Residual strength analysis of laser beam and friction stir welded aluminium panels for aerospace applications*. 2005, Technische Universität Hamburg-Harburg: GKSS Forschungszentrum Geesthacht. p. 212.
11. Russell, M.J., et al., *Recent Developments in the Friction Stir Welding of Titanium Alloys.* Welding in the World, 2008. **52**(9): p. 12-15.
12. Munroe, J., K. Wilkins, and M. Gruber, *Integral Airframe Structures (IAS)---Validated Feasibility Study of Integrally Stiffened Metallic Fuselage Panels for Reducing Manufacturing Costs*. 2000, NASA Langley Technical Report Server.
13. Chen, C.-S., P.A. Wawrzynek, and A.R. Ingraffea, *Residual Strength Prediction of Aircraft Fuselages Using Crack-Tip Opening Angle Criterion.* AIAA Journal, 2002. **40**(3): p. 566-575.
14. Brocks, W., K.-H. Schwalbe, and U. Zerbst, *Structural integrity of thin-walled structures.* Adv. Eng. Mater., 2006. **8**(5): p. 319-328.
15. Lua, J., et al., *Curvilinear Crack Growth and Remaining Life Prediction of Aluminum Weldment Using X-FEM*, in *49th AIAA/ASME/ASCE/AHS/ASC Structures, Structural Dynamics, and Materials Conference*. 2008, American Institute of Aeronautics and Astronautics.
16. Schwalbe, K.-H., I. Scheider, and A. Cornec, *Guidelines for Applying Cohesive Models to the Damage Behaviour of Engineering Materials and Structures*. SpringerBriefs in Applied Sciences and Technology. 2013, Berlin, Heidelberg: Springer Berlin Heidelberg. 89.
17. Barbini, A., J. Carstensen, and J.F. dos Santos, *Influence of a non-rotating shoulder on heat generation, microstructure and mechanical properties of dissimilar AA2024/AA7050 FSW joints.* Journal of Materials Science & Technology, 2018. **34**(1): p. 119-127.
18. Barbini, A., J. Carstensen, and J.F. Dos Santos, *Influence of Alloys Position, Rolling and Welding Directions on Properties of AA2024/AA7050 Dissimilar Butt Weld Obtained by Friction Stir Welding.* Metals, 2018. **8**(4): p. 202.
19. Jain, M., D.J. Lloyd, and S.R. MacEwen, *Hardening laws, surface roughness and biaxial tensile limit strains of sheet aluminium alloys.* International Journal of Mechanical Sciences, 1996. **38**(2): p. 219-232.
20. Zhang, Z.L., et al., *Determining material true stress-strain curve from tensile specimens with rectangular cross-section.* Int. J. Solids Struct., 1999. **36**: p. 3497-3516.
21. Scheider, I., W. Brocks, and A. Cornec, *Procedure for the determination of true stress-strain curves from tensile tests with rectangular cross-section specimens.* Trans. ASME, J. Eng. Mater. Techn., 2004. **126**: p. 1-7.

22. Reynolds, A.P. and F. Duvall, *Digital image correlation for determination of weld and base metal constitutive behavior.* Welding Research Supplement, 1999: p. 355-s-360-s.
23. Community", T.S. *Optimization and Root Finding (scipy.optimize)*. 17.5.2019 20.5.2019]; Available from: https://docs.scipy.org/doc/scipy/reference/optimize.html.
24. Scheider, I. and W. Brocks, *Cohesive elements for thin-walled structures.* Comput. Mater. Sci., 2006. **37**: p. 101-109.
25. Scheider, I. and W. Brocks, *Residual strength prediction of a complex structure using crack extension analyses.* Eng. Fract. Mech., 2008. **75**: p. 4001-4017.
26. Scheider, I., et al., *Crack propagation analyses with CTOA and cohesive model: Comparison and experimental validation.* Eng. Fract. Mech., 2006. **73**: p. 252-263.